Entangled unique coherent line in the ground-state phase diagram of the spin-1/2 XX chain model with three-spin interaction

F. Khastehdel Fumani [1], S. Mahdavifar [2] and K. Afrousheh [3,*]

[1]*Department of Basic Sciences, Langarud Branch, Islamic Azad University, 4471311127 Langarud, Iran*

[2]*Department of Physics, University of Guilan, 41335-1914 Rasht, Iran*

[3]*Department of Physics, Kuwait University, P.O. Box 5969, 13060 Safat, Kuwait*

(Received 3 September 2023; revised 27 February 2024; accepted 19 March 2024; published 18 April 2024)

Entangled spin coherent states are a type of quantum states that involve two or more spin systems that are correlated in a nonclassical way. These states can improve metrology and information processing, as they can surpass the standard quantum limit, which is the ultimate bound for precision measurements using coherent states. However, finding entangled coherent states in physical systems is challenging because they require precise control and manipulation of the interactions between the modes. In this work we show that entangled unique coherent states can be found in the ground state of the spin-1/2 XX chain model with three-spin interaction, which is an exactly solvable model in quantum magnetism. We use the spin squeezing parameter, the l_1-norm of coherence, and the entanglement entropy as tools to detect and characterize these unique coherent states. We find that these unique coherent states exist in a gapless spin liquid phase, where they form a line that separates two regions with different degrees of squeezing. We call this line the entangled unique coherent line, as it corresponds to the almost maximum entanglement between two halves of the system. We also study the critical scaling of the spin squeezing parameter and the entanglement entropy versus the system size.

DOI: 10.1103/PhysRevE.109.044142

I. INTRODUCTION

Quantum coherence is a quantum phenomenon that allows quantum systems to exist in superpositions of states, which means that they can be in more than one state at the same time [1–4]. This enables quantum interference, which is the constructive or destructive combination of quantum waves, such as light or matter waves. Quantum coherence and interference are essential features of quantum physics that distinguish it from classical physics. They also have many applications in fields such as quantum optics, quantum information, quantum metrology, and quantum computing.

A way to quantify quantum coherence is to use the l_1-norm of coherence, which is a theoretical measure of coherence that is based on the concept of quantum distinguishability [5,6]. The l_1-norm of coherence is defined as the sum of the absolute values of the off-diagonal elements of the density matrix of the quantum system. The off-diagonal elements of the density matrix indicate the coherence between different basis states of the system. The l_1-norm of coherence can be used to compare the coherence of different quantum ground states of complicated many-body systems. The l_1-norm of coherence is defined as

$$C_{l_1}(\hat{\rho}) = \sum_{i \neq j} |\rho_{ij}|, \tag{1}$$

where $\hat{\rho}$ is the density operator of the quantum state and $\rho_{ij} = \langle \psi_i | \hat{\rho} | \psi_j \rangle$. Here $\{|\psi_m\rangle\}$ are basis kets of the Hilbert space. It is important to note that density matrices that are diagonal in this basis are considered incoherent.

Coherent states are also defined based on the spin-squeezing parameter (SSP). Spin squeezing is a way of reducing the quantum noise in one direction of the collective spin of a system of particles, making it more sensitive to rotations around that axis [7–10]. This can improve the accuracy of measurements and the performance of quantum information protocols. Spin squeezing has many applications in quantum physics, such as quantum metrology [3,11–15], which is the science of measuring physical quantities with quantum-enhanced precision; quantum entanglement [16–22], which is the phenomenon of having quantum correlations between two or more systems; and quantum phase transitions [3,23–32], which are abrupt changes in the properties of a system due to quantum fluctuations.

The SSP measures how much the quantum noise in one direction of the total spin of a system of particles is reduced and is given by the Kitagawa-Ueda parameter as [8]

$$\xi_s^2 = \frac{4(\Delta J_{\vec{n}_\perp})^2}{N}, \tag{2}$$

where $\vec{n}_\perp$ is the axis perpendicular to the average spin direction $\vec{n}_0$ and the variance $(\Delta J)^2$ is minimized. The total spin components J_α of N particles satisfy $[J_\alpha, J_\beta] = i\hbar J_\gamma$, where α, β, γ are cyclic permutations of x, y, z. Another SSP is $\xi_R^2 = \frac{N(\Delta J_{\vec{n}_\perp})^2}{|\langle J_{\vec{n}} \rangle|^2}$, which was introduced by Wineland *et al.* [9]. For spin systems with a well-defined mean spin direction and many particles, the Kitagawa-Ueda parameter is a good way to measure spin squeezing. On the other hand, the parameter

*k.afrousheh@ku.edu.kw

from Wineland *et al.* is good for spin systems that are affected by SU(2) rotations and have few particles. A nonsqueezed state has $\xi_s^2 > 1$ and a spin squeezed state has $\xi_s^2 < 1$. In this context, a coherent state is characterized by $\xi_s^2 = 1$ and we call it a unique coherent state.

Thus, squeezed states and unique coherent states are two types of quantum states that have different uncertainties in the angular momentum of a system of particles. Squeezed states have less noise in one direction, but more noise in the other direction. Unique coherent states have equal noise in all directions. In other words, unique coherent states have the smallest possible uncertainty for any pair of perpendicular components of the angular momentum, such as J_x and J_y.

The coherent states are also divided into the entangled and nonentangled states [2,33–38]. The entangled states are states that cannot be described by the individual properties of their components, but only by their correlations. Entangled coherent states have some interesting properties and applications in quantum information. They can be used to test the violation of local realism, which is the assumption that physical reality is independent of observation and that information cannot travel faster than light. They can also be used for quantum teleportation, which is the process of transferring the quantum state of one system to another without sending any physical particles. Furthermore, they can be used for quantum dense coding, which is the process of sending more than one classical bit of information using a single quantum bit.

As we have mentioned, the SSP is a useful tool to study the entanglement and quantum criticality of complex many-body systems at zero temperature, which has been a topic of great interest in recent years. Some of the interesting results are that the SSP can be minimal at the critical point even when another entanglement measure, the concurrence, is not maximal [23] and that there can be a phase where the ground state is entangled but not spin squeezed [24]. The scaling behavior of the SSP with system size at the quantum critical point has also been explored in various models [39–42].

In this paper, we investigate the SSP in the ground-state phase diagram of the one-dimensional (1D) spin-1/2 XX model with three-spin interaction (TSI). This is a type of cluster interaction, where a group of spins interacts collectively. In particular, TSI is when three spins are coupled by a term that depends on the product of their spin components [43–60]. The TSI can cause frustration, entanglement, and quantum phase transitions in spin systems. We study how such interactions affect the ground-state phase diagram of the 1D spin-1/2 XX model by looking at the SSP, the l_1-norm of coherence, and the entanglement entropy (EE). We find that there is an entangled unique coherent line in the gapless spin liquid phase [see Fig. 1(b)]. The entangled unique coherent line is a concept that refers to a type of quantum state that is both entangled and coherent. By using the quantum correlations and superpositions of the system, an entangled unique coherent line can improve the efficiency and reliability of quantum protocols.

The paper is structured as follows. In the next section we present the model and tools. In Sec. III we show our results on the SSP, the l_1-norm of coherence, and the EE. We summarize and discuss our results in Sec. IV.

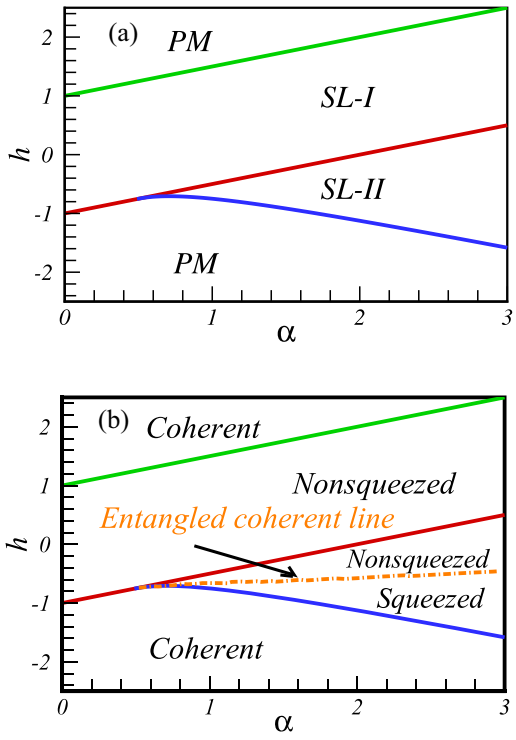

FIG. 1. (a) Schematic picture of the ground-state phase diagram of the spin-1/2 XX chain model with three-spin interaction [44]. (b) Same as in (a) but from the viewpoint of the spin squeezing parameter and the entanglement entropy.

II. MODEL AND TOOLS

The Hamiltonian of the spin-1/2 XX chain model with TSI interaction in the presence of a uniform magnetic field is defined as

$$\mathcal{H} = -J\sum_{n=1}^{N}\left(S_n^x S_{n+1}^x + S_n^y S_{n+1}^y\right) - J^*\sum_{n=1}^{N} S_{n+1}^z\left(S_n^x S_{n+2}^x + S_n^y S_{n+2}^y\right) - Jh\sum_{n=1}^{N} S_n^z, \quad (3)$$

where S_n is the spin operator on the nth site, $J > 0$ is the ferromagnetic exchange coupling, J^* and h are the strength of the TSI and the uniform magnetic field, respectively, N is the system size (or number of spins), and we consider the periodic boundary condition $S_{N+1}^{\mu} = S_1^{\mu}$ ($\mu = x, y, z$). Here $\alpha = \frac{J^*}{J}$ is defined without loss of generality.

The exact ground-state phase diagram of this model is known [44]. When $h = 0$, there is a second-order quantum phase transition at $\alpha_c = 2$ between two gapless spin liquid (SL) phases SL-I and SL-II. This quantum phase transition corresponds to the doubling of Fermi points in the spinless fermions representation. The magnetic and thermodynamic properties of the system show anomalous behavior at this critical point. The critical index of the transverse spin-spin correlation function also changes at this point. When $h \neq 0$, a spin-saturated paramagnetic (PM) phase appears in the ground-state phase diagram as shown in Fig. 1(a). There are three critical lines: $h_c = 1 + \frac{\alpha}{2}$, which separates PM and SL-I

phases; $h_c = -(1 - \frac{\alpha}{2})$, which separates PM and SL-I phases in the region $\alpha \leqslant 0.5$ and also separates SL-I and SL-II phases in the region $\alpha > 0.5$; and $h_c = -\frac{2\alpha^2+1}{4\alpha}$, which separates PM and SL-II phases in the region $\alpha > 0.5$. It should be noted that quantum correlations between pair spins (as the quantum discord) in the SL-I phase are stronger than in the SL-II phase [50,57].

The Hamiltonian can be diagonalized. First, applying the Jordan-Wigner transformation

$$S_n^+ = c_n^\dagger \exp\left(i\pi \sum_{m=1}^{n-1} c_m^\dagger c_m\right),$$
$$S_n^- = \exp\left(-i\pi \sum_{m=1}^{n-1} c_m^\dagger c_m\right) c_n,$$
$$S_n^z = c_n^\dagger c_n - \frac{1}{2}, \tag{4}$$

where $c_n^\dagger$ and c_n are the fermionic operators, the fermionized form of the Hamiltonian is obtained as

$$\mathcal{H} = -\frac{J}{2}\sum_{n=1}^{N}(c_n^\dagger c_{n+1} + c_{n+1}^\dagger c_n)$$
$$-\frac{J^*}{4}\sum_{n=1}^{N}(c_n^\dagger c_{n+2} + c_{n+2}^\dagger c_n) - Jh\sum_{n=1}^{N} c_n^\dagger c_n. \tag{5}$$

Then performing a Fourier transformation $c_n = \sum_k e^{-ikn} c_k$ yields the diagonalized Hamiltonian

$$\mathcal{H} = \sum_k \varepsilon_k\, c_k^\dagger c_k, \tag{6}$$

with the energy spectrum

$$\varepsilon_k = -J\left(h + \cos(k) - \frac{\alpha}{2}\cos(2k)\right). \tag{7}$$

It should be noted that the summation in Eq. (6) runs over $k = 2\pi m/N$, with $m = 0, \pm 1, \ldots, \pm\frac{1}{2}(N-1)$ and $m = 0, \pm 1, \ldots, \pm(\frac{1}{2}N - 1)$, $\frac{1}{2}N$ for N odd and N even, respectively (having imposed periodic boundary conditions on the Jordan-Wigner fermions). In the thermodynamic limit $N \to \infty$, the ground state of the system corresponds to the configuration where all the states with $\varepsilon_k < 0$ are filled and those with $\varepsilon_k > 0$ are empty.

Considering the symmetries of the model as the unbroken Z_2 invariance for finite N implies that

$$\langle J_x\rangle = \langle J_y\rangle = 0, \tag{8}$$

and similarly

$$\langle J_\alpha J_z\rangle = \langle J_z J_\alpha\rangle = 0, \quad \alpha = x, y. \tag{9}$$

The magnetization for $h > 0$ is always along the z axis, with full polarization developing in the PM phase. As a result, $J_{\vec{n}_\perp} = \cos(\Omega)J_x + \sin(\Omega)J_y$, with Ω to be chosen to minimize

$$(\Delta J_{\vec{n}_\perp})^2 = \langle (J_{\vec{n}_\perp})^2\rangle - \langle J_{\vec{n}_\perp}\rangle^2$$
$$= \langle [\cos(\Omega)J_x + \sin(\Omega)J_y]^2\rangle. \tag{10}$$

We can easily show that

$$\xi_s^2 = \frac{2}{N}\min_\Omega\left[\langle J_x^2 + J_y^2\rangle + \cos(2\Omega)\langle J_x^2 - J_y^2\rangle\right.$$
$$\left. + \sin(2\Omega)\langle J_x J_y + J_y J_x\rangle\right]$$
$$= \frac{2}{N}\left(\langle J_x^2 + J_y^2\rangle - \sqrt{\langle J_x^2 - J_y^2\rangle^2 + \langle J_x J_y + J_y J_x\rangle^2}\right). \tag{11}$$

Finally, using the definition of the total spin of the particles, the SSP is obtained as

$$\xi_s^2 = 1 + 2\sum_{n=1}^{N-1}\left(G_n^{xx} + G_n^{yy}\right)$$
$$-2\sqrt{\left(\sum_{n=1}^{N-1}\left(G_n^{xx} - G_n^{yy}\right)\right)^2 + \left(\sum_{n=1}^{N-1}\left(G_n^{xy} + G_n^{yx}\right)\right)^2}, \tag{12}$$

where $G_n^{\alpha\beta}$ denotes the two-point correlation function. Introducing $A_n = a_n^\dagger + a_n$ and $B_n = a_n^\dagger - a_n$, a direct calculation shows that

$$G_n^{xx} = \langle S_1^x S_{1+n}^x\rangle = \frac{1}{4}\langle B_1 A_2 B_2 \cdots A_n B_n A_{n+1}\rangle,$$
$$G_n^{yy} = \langle S_1^y S_{1+n}^y\rangle = \frac{(-1)^n}{4}\langle A_1 B_2 A_2 \cdots B_n A_n B_{n+1}\rangle,$$
$$G_n^{xy} = \langle S_1^x S_{1+n}^y\rangle = \frac{-i}{4}\langle B_1 A_2 B_2 \cdots A_n B_n B_{n+1}\rangle,$$
$$G_n^{yx} = \langle S_1^y S_{1+n}^x\rangle = \frac{i(-1)^n}{4}\langle A_1 B_2 A_2 \cdots B_n A_n A_{n+1}\rangle. \tag{13}$$

These equations may be written in the generic form

$$G_n^{\alpha\beta} = D_n^{\alpha\beta}\langle \phi_1\phi_2\phi_3\cdots\phi_{2n-2}\phi_{2n-1}\phi_{2n}\rangle, \tag{14}$$

with

$$D_n^{xx} = \frac{1}{4}, \quad D_n^{yy} = \frac{(-1)^n}{4},$$
$$D_n^{xy} = \frac{-i}{4}, \quad D_n^{yx} = \frac{i(-1)^n}{4}, \tag{15}$$

where each operator ϕ_j, $j = 1, 2, \ldots, 2n$, is identified with either an A_n or a B_n operator. Using the Wick theorem [61], the $2n$-point functions can be expressed as Pfaffians

$$G_n^{\alpha\beta} = D_n^{\alpha\beta}\,\mathrm{pf}\begin{pmatrix} \langle\phi_1\phi_2\rangle & \langle\phi_1\phi_3\rangle & \langle\phi_1\phi_4\rangle & \cdots & \langle\phi_1\phi_{2n}\rangle \\ & \langle\phi_2\phi_3\rangle & \langle\phi_2\phi_4\rangle & \cdots & \langle\phi_2\phi_{2n}\rangle \\ & & \langle\phi_3\phi_4\rangle & \cdots & \langle\phi_3\phi_{2n}\rangle \\ & & & \ddots & \vdots \\ & & & & \langle\phi_{2n-1}\phi_{2n}\rangle \end{pmatrix}, \tag{16}$$

where we have written the skew-symmetric matrix in the standard abbreviated form.

One way to study fermionic systems is to use the correlation matrix, which captures the single-particle properties and the correlations of the many-body wave function [62–66]. The ground-state density matrix is another matrix that shows the probability distribution of the system states when the energy is

minimized. The same ground state gives rise to both matrices, and they have the same eigenvalues. However, this does not mean that the density matrix and the correlation matrix have the same off-diagonal elements. The l_1-norm of coherence is the sum of absolute values of the off-diagonal elements of the density matrix. A nonzero l_1-norm means that the ground state has coherence. However, the exact value of the l_1-norm is not important, only the nonzero property. That is why we use the sum of absolute values of off-diagonal elements of the correlation matrix to approximate the l_1-norm of coherence in the basis of the z component of the total spin. Next we show that this approximation reveals some key features of the system.

The correlation matrix of the ground state is a matrix of expectation values of fermionic operators

$$\rho_N = \begin{pmatrix} \langle c_1^\dagger c_1\rangle & \cdots & \langle c_1^\dagger c_N\rangle & \langle c_1^\dagger c_1^\dagger\rangle & \cdots & \langle c_1^\dagger c_N^\dagger\rangle \\ \langle c_2^\dagger c_1\rangle & \cdots & \langle c_2^\dagger c_N\rangle & \langle c_2^\dagger c_1^\dagger\rangle & \cdots & \langle c_2^\dagger c_N^\dagger\rangle \\ \vdots & \vdots & \vdots & \vdots & \vdots & \vdots \\ \langle c_l^\dagger c_1\rangle & \cdots & \langle c_l^\dagger c_N\rangle & \langle c_l^\dagger c_1^\dagger\rangle & \cdots & \langle c_l^\dagger c_N^\dagger\rangle \\ \langle c_1 c_1\rangle & \cdots & \langle c_1 c_N\rangle & \langle c_1 c_1^\dagger\rangle & \cdots & \langle c_1 c_N^\dagger\rangle \\ \langle c_2 c_1\rangle & \cdots & \langle c_2 c_N\rangle & \langle c_2 c_1^\dagger\rangle & \cdots & \langle c_2 c_{lN}^\dagger\rangle \\ \vdots & \vdots & \vdots & \vdots & \vdots & \vdots \\ \langle c_l c_1\rangle & \cdots & \langle c_l c_N\rangle & \langle c_l c_1^\dagger\rangle & \cdots & \langle c_l c_N^\dagger\rangle \end{pmatrix}, \tag{17}$$

where

$$\langle c_n^\dagger c_m\rangle = \frac{1}{N}\sum_{k\in\lambda} e^{i[k(m-n)]},$$
$$\langle c_n^\dagger c_m^\dagger\rangle = 0, \tag{18}$$

with λ denoting a k-space region with $\varepsilon_k < 0$. From this correlation matrix, the l_1-norm of coherence is approximated as

$$C_{l_1}(\hat{\rho}) \simeq \sum_{m\neq n} |\langle c_n^\dagger c_m\rangle|. \tag{19}$$

We can also easily find

$$\langle A_n A_m\rangle = \delta(m-n),$$
$$\langle B_n B_m\rangle = -\delta(m-n),$$
$$\langle A_n B_m\rangle = \delta(m-n) - \frac{2}{N}\sum_{k\in\lambda}\cos[k(m-n)],$$
$$\langle B_n A_m\rangle = -\delta(m-n) + \frac{2}{N}\sum_{k\in\lambda}\cos[k(m-n)]. \tag{20}$$

It is known that when a quantum state is entangled the entropy arises. This entropy is called entanglement entropy [67]. In fact, the EE is a measure of the total entanglement of bipartite pure states and it is widely used in quantum information theory. It is defined as the von Neumann entropy of a reduced density matrix of a subsystem [68–73]. For a bipartite system, EE in the pure ground state $|\psi\rangle$, with the density matrix $\rho = |\psi\rangle\langle\psi|$, is defined as the von Neumann entropy of subsystem A as

$$S_A = -\mathrm{Tr}[\rho_A \log_2(\rho_A)], \tag{21}$$

where

$$\rho_A = \mathrm{Tr}_B(\rho) \tag{22}$$

is the reduced density matrix of A obtained by tracing over the rest of the system B. The EE usually grows like the boundary area of the subsystem A and not like its volume, which is different from an expected extensive behavior. This is known as the area law for the EE and has been studied extensively in recent years. Noncritical ground states of spin chains with a finite correlation length have a constant EE. At a quantum critical point, when subsystem A is a finite interval of length l, the EE slightly violates the area law by a logarithmic correction as $S_A(l) \sim \frac{c_{\mathrm{eff}}}{3}\log(l)$, where c_{eff} is the central charge [74,75]. The EE of a finite block of l sites in an infinite system of free spinless fermions can be computed by [62,66]

$$S_A = -\sum_{\gamma=1}^{2l} C_\gamma \log(C_\gamma), \tag{23}$$

where C_γ is one of the $2l$ eigenvalues of the correlation matrix ρ_l.

III. RESULTS

We investigated how the SSP depends on the TSI and the magnetic field in the ground state of our chain system. We considered different chain sizes up to $N = 1000$ and calculated the SSP for all ground-state phases shown in Fig. 1(a). Figure 2 shows the results for different chain sizes $N = 500$, 700, and 1000. Without the TSI, Fig. 2(a) reveals the quantum critical points in the SSP. One of the eigenstates of the z component of the total spin is the ground state in the PM phase, which gives $G_n^{xx} = G_n^{yy} = 0$ and thus $\xi_s^2 = 1$. However, the ground state is strongly nonsqueezed in the SL-I phase. An increasing size effect is seen in the SL-I phase. With the TSI, $\alpha = 2.0$, Fig. 2(b) displays three critical points, in particular between the SL-I and SL-II phases. The ground state becomes squeezed when entering the SL-II phase from the PM phase and reaches a coherent state at a certain value of the magnetic field. Beyond that value, the ground state is nonsqueezed again in the SL-II phase. It should be noted that there is no size effect on this squeezed region. A sudden jump in the SSP occurs when transitioning to the SL-I phase, where the ground state is strongly nonsqueezed. Figure 2(c) shows the density plot of the SSP as a function of the magnetic field and the TSI interaction for a chain size $N = 200$. The SSP indicates that the ground state is coherent in the PM phase, which is typical for saturated spin phases and is squeezed in a part of SL-II phase bordered between a saturated critical line and a unique coherent line. These results also show that the minimum uncertainty does not always occur at the quantum critical lines. However, in the SL-II phase, there is a line of coherence with $\xi_s^2 = 1$.

To better understand the nature of the unique coherent line, we have computed the scaled l_1-norm of coherence (C_{l_1}/N) as a function of TSI and magnetic field. We present the results for $\alpha = 2.0$ and a chain size $N = 1000$ in Fig. 2(d). We find

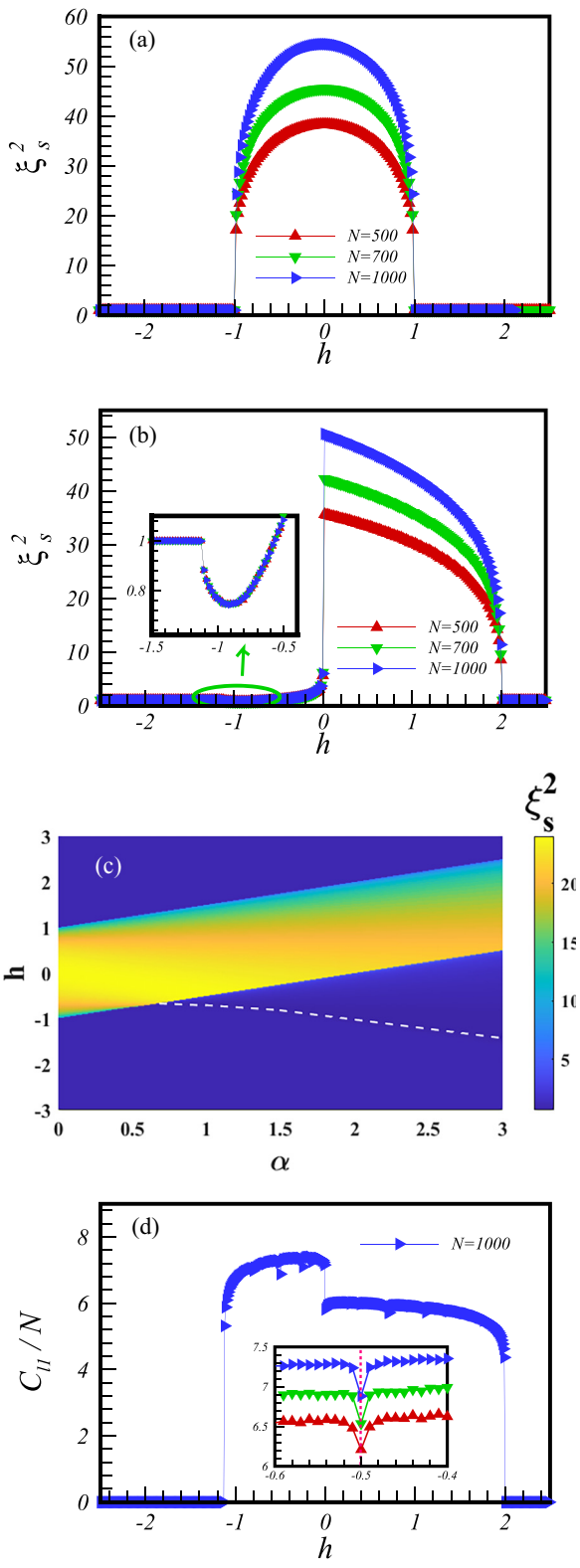

FIG. 2. The SSP as a function of the magnetic field for three different chain sizes $N = 500$, 700, and 1000 (a) in the absence of TSI, $\alpha = 0$, and (b) in the presence of TSI, $\alpha = 2$. (c) Density plot of the SSP for a chain size $N = 200$. (d) The l_1-norm of coherence as a function of the magnetic field for a chain size $N = 1000$ and $\alpha = 2$. The inset shows the local minima at exactly the coherent point for three chains lengths $N = 500$, 700, and 1000.

that the system has a coherent ground state in the gapless SL-II and SL-I phases. However, the coherence is stronger in the SL-II phase than in the SL-I phase. Moreover, the ground state is not coherent in the polarized PM phases, as expected. The coherence function has a discontinuity at the quantum critical points, where it jumps to a higher value, signaling the quantum phase transitions. As we mentioned, when $\xi_s^2 = 1$, the ground state is a unique coherent state with equal noise in magnetization in all directions. Therefore, we investigated the coherence function to identify these special coherent states. We show the results in the inset of Fig. 2(d) for different chain sizes $N = 500$, 700, and 1000 at $\alpha = 2.0$. Interestingly, we observe a minimum in the coherence function at a specific magnetic field value $h_{\rm coh} = -0.5$. Thus, we conclude that the coherence function can effectively detect these unique coherent states with $\xi_s^2 = 1$, as they correspond to local minima in the coherence measurement. Besides the one at $h_{\rm coh} = -0.5$, there are other minima in the coherence function in Fig. 2(d). We believe that these minima are related to the quantum correlations, which are the nonclassical correlations that a quantum system can show (see the Appendix).

We are interested in the nature of the system's ground state, especially the coherent line that we mentioned before. To study this, we use the EE as a tool [76–79]. The EE measures how much information we lose when we look at only part of the system and ignore the rest. It can also tell us how entangled different regions of the system are and how this changes across different phases and quantum phase transitions. Entanglement is important for quantum metrology, which uses Ramsey interferometers to measure physical quantities with high precision. By controlling the interactions among the particles, we can create entangled states that improve the interferometric sensitivity. The EE can help us distinguish between different types of entangled states. We split the system into two equal parts and calculate the EE of one part $S_A(l = N/2)$. For systems with a gap, this EE quickly reaches a constant value, which follows the area law. When there is no TSI, $\alpha = 0$, the system becomes the isotropic XX model, which has a quantum critical point with a central charge of $c_{\rm eff} = 1$ [64,80,81].

We show our results on $S_A(l = N/2)$ in Fig. 3. When $\alpha = 0$, the two equal parts of the system are not entangled in the PM phase. Without the TSI, the system is entangled across the SL-I phase, as Fig. 3(a) shows for chain sizes $N = 500$, 700, and 1000. However, the entanglement drops to zero at the quantum critical points that separate the PM and SL phases. With the TSI, the quantum critical points are visible in the EE as dips in Fig. 3(b). The entanglement is stronger in the SL-II phase than in the SL-I phase, which agrees with the opposite behavior of the SSP. The entanglement of the system is nearly maximal at the coherent point where $\xi_s^2 = 1$. This shows that the unique coherent ground state is not an eigenstate of J_z. Figure 3(c) shows the density representation of the EE versus the TSI interaction and the magnetic field for a chain size $N = 200$. Our results show that the EE in the ground-state phase diagram is a useful way of exploring how the entanglement between different regions varies across different phases and phase transitions.

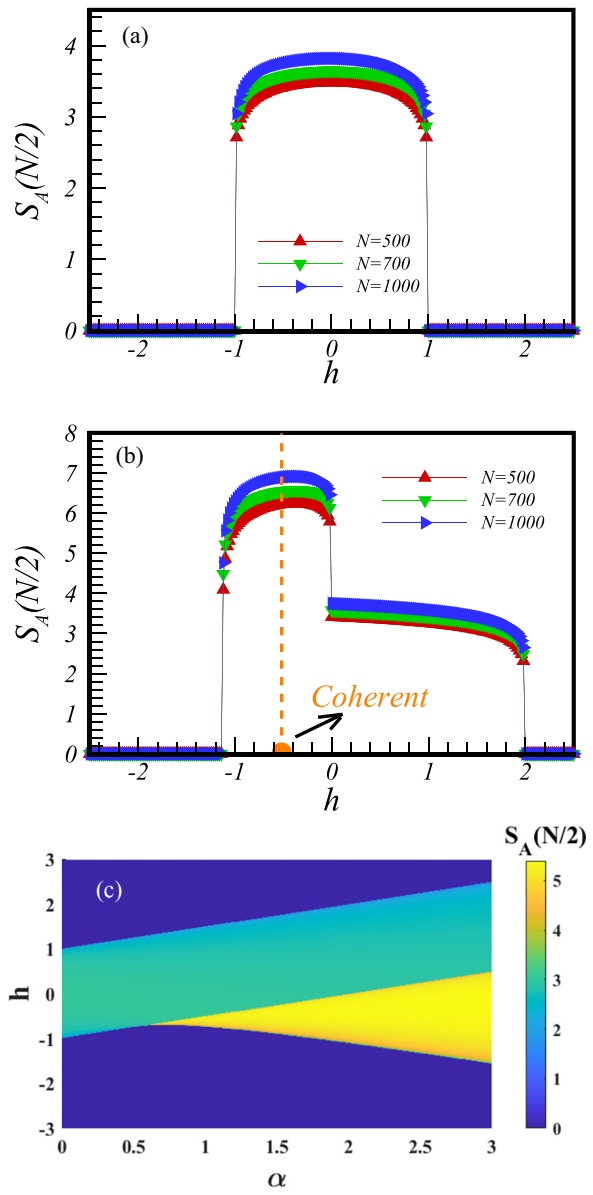

FIG. 3. The EE as a function of the magnetic field for three different chain sizes $N = 500$, 700, and 1000 (a) in the absence of TSI, $\alpha = 0$, and (b) in the presence of TSI, $\alpha = 2$. (c) Density plot of the EE parameter for a chain size $N = 200$.

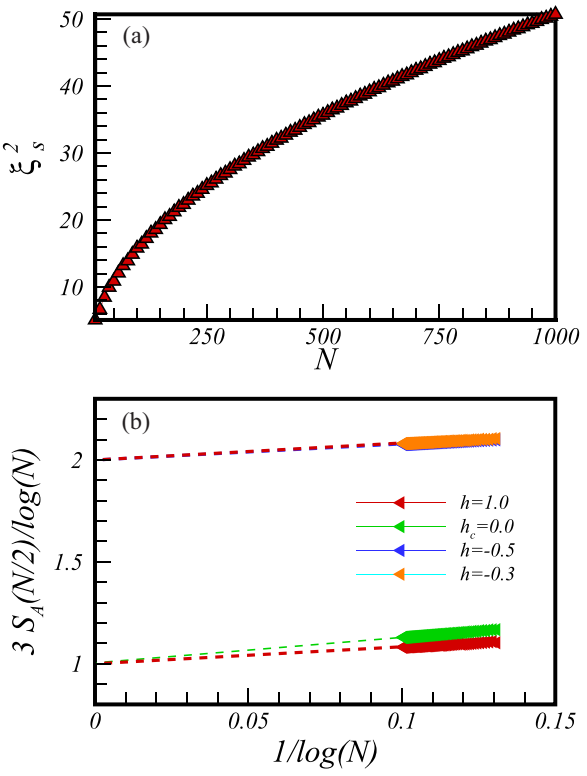

FIG. 4. (a) The SSP with respect to the size of the system on the critical line separating SL-I and SL-II phases for $\alpha = 0$ and $h_c = 0$. (b) Linear fit of the form $Y = mX + b$ applied to the function $3S_A(N/2)/\log(N) = c_{\text{eff}} + m/\log(N)$ on the critical line separating SL-I and SL-II phases and also in these gapless phases for for $\alpha = 2$. Chain sizes are considered up to $N = 1000$. Logarithms are calculated using base 2.

A system near a critical point, where it undergoes a phase transition, exhibits scaling behavior, which reflects its self-similarity and universality. This behavior is manifested by the appearance of scaling laws and functions, which involve important parameters such as scaling exponents and variables. These scaling laws and functions are essential for describing how the system's physical properties vary as it approaches a critical point. They reveal the critical behavior of the system, emphasizing the common features and patterns that are independent of specific details, making them useful tools in the study of phase transitions and critical phenomena. We study how the system size affects the SSP and the EE functions in the following. We analyze the scaling behavior of these quantities, which is crucial for revealing the universal features related to quantum phase transitions and quantum criticality. The practical usefulness of these scaling analyses in quantifying quantum phase transitions is a fascinating and active research topic.

The SSP scaling has important applications in quantum metrology and quantum sensing. These fields deal with quantum measurements in spin systems, which have two fundamental limits on their precision: the standard limit and the Heisenberg limit. The standard limit, also known as the shot-noise limit or standard quantum limit, is the precision that can be achieved using coherent or uncorrelated spin states [82,83]. It depends on the number of spins N as $1/\sqrt{N}$. The Heisenberg limit, also known as the ultimate limit or quantum Cramér-Rao bound, is the precision that can be achieved using squeezed or entangled spin states. It depends on the number of spins N as $1/N$ [11,84,85]. The Heisenberg limit is the highest possible precision for any quantum state and it beats the standard limit by a factor of $1/\sqrt{N}$.

We show our scaling results in Fig. 4, focusing on the SSP and the EE of the ground state of the system at the critical points and the gapless SL-I and SL-II phases. Our results reveal that the SSP is not scalable on the critical lines separating the PM and the gapless phases. On the critical line separating the gapless SL-I and SL-II phases, we see a square root divergence $\xi_s^2 \propto \sqrt{N}$ of the SSP with increasing

system size in Fig. 4(a). Moreover, we find the same square root behavior in the gapless SL-I phase, which indicates that the SL-I phase is a critical region from the SSP perspective. This can be related to the scaling behavior of the transverse two-point correlation functions G_n^{xx} and G_n^{yy}. It was shown that in the SL-I phase the transverse two-point correlation functions behaves as [44]

$$G_n^{xx} = G_n^{yy} = \frac{A(\alpha)}{n^{1/2}} + \frac{B(\alpha)\cos(2k_F n)}{n^{5/2}}, \tag{24}$$

where $A(\alpha)$ and $B(\alpha)$ are smooth functions of TSI. In this region, the SSP can be rewritten as

$$\xi_s^2 = 1 + 4\sum_{n=1}^{N-1}\left(\frac{A(\alpha)}{n^{1/2}} + \frac{B(\alpha)\cos(2k_F n)}{n^{5/2}}\right). \tag{25}$$

By considering only the first term in the thermodynamic limit, it can be shown that $\xi_s^2 \sim 1 + 8A(\alpha)\sqrt{N}$.

Finally, we studied the scaling of EE on the critical lines and the gapless phases of the model. We used linear fits to the function $3S_A(N/2)/\log(N) = c_{\text{eff}} + m/\log(N)$ for chain sizes up to $N = 1000$, as shown in Fig. 4(b) for $\alpha = 2.0$, to extrapolate the central charge in the thermodynamic limit. We did not observe any deviation from the area law in the PM phase and on the critical lines separating the PM and the gapless phases since in the paramagnetic phase the system is in a disordered state where the spins are randomly aligned and do not exhibit long-range order. The system is also gapped, meaning that there is a finite energy gap between the ground state and the first excited state. Therefore, the paramagnetic phase satisfies the conditions for the area law of entanglement entropy and no deviation is expected. On the critical line separating the gapless SL-I and SL-II phases, we found the central charge to be $c_{\text{eff}} = 1.0$, which is the same as for the isotropic spin-1/2 XX chain model. However, from the EE perspective, we found that the SL-I and SL-II phases are critical with different central charges. In particular, in the SL-II phase, we obtained $c_{\text{eff}} = 2.0$, which is twice as large as the SL-I phase. The quantum correlations and the spin-spin correlation patterns in the two gapless phases can explain the difference in the central charge. Figure 3(b) shows that the EE in the SL-II phase is almost double that in the SL-I phase. Also, the transverse spin-spin correlation functions in the SL-II phase decay faster than in the SL-I phase [44].

IV. CONCLUSION

In this paper, we investigated the entanglement properties of the spin-1/2 XX chain model with TSI, which is an exactly solvable model that has a rich ground-state phase diagram consisting of three phases: a gapped PM phase and two gapless SL phases called SL-I and SL-II. We were motivated by the possibility of finding an entangled spin coherent state in this model, which is a special state that does not belong to an eigenstate of J_z. We used three tools to study this model: the SSP, the l_1-norm of coherence, and the EE. The l_1-norm of coherence indicates whether or not the ground state is a superposition of states. The SSP measures how much spin coherence there is in the system, while the EE measures how much entanglement there is between different parts of the system.

First, we computed the SSP for the whole phase diagram and showed that it can detect all the quantum critical lines that separate different phases.

Second, we discovered a unique coherent line in the SL-II phase where the SSP becomes one, which indicates that this line corresponds to the coherent state. We also found that the system is squeezed between this line and another quantum critical line, while it is nonsqueezed in the rest of the SL-II phase and in the SL-I phase. Moreover, we found that the system is more nonsqueezed in the SL-I phase than in the SL-II phase. Additionally, we detected the signature of the mentioned special coherent line as a local minimum in the l_1-norm of coherence.

Third, we divided the system into two equal parts and computed the EE between them. We showed that this quantity can also detect all the quantum critical lines in the phase diagram. Furthermore, we found that the two halves are entangled in both SL phases, but they have almost maximum entanglement on the coherent line. We called this line the entangled unique coherent line. We also presented a density plot of the EE as a function of both the TSI interaction and the magnetic field. We can think of this plot as a map of the entanglement landscape of the system, where different regions have different levels of entanglement. Our results demonstrate that studying this landscape can help us understand how entanglement behaves across different phases and phase transitions in quantum systems.

Fourth, we studied the scaling behavior of the SSP and the EE with respect to the system size. We discovered that the SSP is scalable and has a square root behavior in the gapless SL-I phase and on the critical line separating it from the SL-II phase. We also noticed that the EE does not follow the area law in the entire range of the gapless SL-I and SL-II phases. The central charge in the SL-II phase is twice as large as the SL-I phase.

For future works, we suggest to investigate the effect of thermal noise or dynamical noise on the spin squeezing and coherence of this model, as these factors can limit the performance and sensitivity of the spin-based magnetic sensors [86–90]. We also suggest to study the spin-noise spectroscopy of this model, as this technique can provide insight into the dynamics and fluctuations of the spin system, even in regimes where the macroscopic atomic coherence is lost. We hope that our paper will stimulate further research on the spin squeezing phenomenon and its applications in quantum physics.

APPENDIX

In Fig. 2(d) we observe that the coherence function has multiple minima, not only at $h_{\text{coh}} = -0.5$. We have argued in the main text that these minima reflect the presence of quantum correlations, which are correlations that go beyond the classical realm. In this Appendix we provide the evidence for our argument and demonstrate our findings.

We calculated the concurrence and the one-tangle. The concurrence is a measure of quantum entanglement, which is the phenomenon of two or more quantum systems being correlated in such a way that their quantum states cannot be

described independently. Concurrence quantifies the degree of entanglement between two spin-1/2 particles [91–93].

The concurrence between two spins at site n and m can be achieved from the corresponding reduced density matrix $\rho_{n,m}$ as [94]

$$\rho_{n,m} = \begin{pmatrix} X^{+}_{n,m} & 0 & 0 & 0 \\ 0 & Y^{+}_{n,m} & Z^{*}_{n,m} & 0 \\ 0 & Z_{n,m} & Y^{-}_{n,m} & 0 \\ 0 & 0 & 0 & X^{-}_{n,m} \end{pmatrix}, \tag{A1}$$

where

$$\begin{aligned} X^{+}_{n,m} &= \langle P^{\uparrow}_{n} P^{\uparrow}_{m} \rangle, \\ Y^{+}_{n,m} &= \langle P^{\uparrow}_{n} P^{\downarrow}_{m} \rangle, \\ Y^{-}_{n,m} &= \langle P^{\downarrow}_{n} P^{\uparrow}_{m} \rangle, \\ Z_{n,m} &= \langle S^{+}_{n} S^{-}_{m} \rangle, \\ X^{-}_{n,m} &= \langle P^{\downarrow}_{n} P^{\downarrow}_{m} \rangle, \end{aligned} \tag{A2}$$

with $P^{\uparrow} = \frac{1}{2} + S^{z}$, $P^{\downarrow} = \frac{1}{2} - S^{z}$, and $S^{\pm} = S^{x} \pm iS^{y}$. It should be noted that the matrix is written in the standard basis $\{|\uparrow\uparrow\rangle, |\uparrow\downarrow\rangle, |\downarrow\uparrow\rangle, |\downarrow\downarrow\rangle\}$ and its elements are expectation values on the ground state of the system. By using the Jordan-Wigner transformations, the density matrix elements can be obtained as

$$\begin{aligned} X^{+}_{n,m} &= \langle n_n n_m \rangle, \\ X^{-}_{n,m} &= \langle 1 - n_n - n_m + n_n n_m \rangle, \\ Y^{+}_{n,m} &= \langle n_n (1 - n_m) \rangle, \\ Y^{-}_{n,m} &= \langle n_n (1 - n_m) \rangle, \\ Z_{n,m} &= \langle c^{\dagger}_{n} c_m \rangle. \end{aligned} \tag{A3}$$

We have used the occupation number operator $n_i = c^{\dagger}_{i} c_i$ in the above expressions. Finally, the concurrence is obtained as

$$\mathcal{C}_{n,m} = \max\{0, 2(|Z_{n,m}| - \sqrt{X^{+}_{n,m} X^{-}_{n,m}})\}. \tag{A4}$$

Here we have studied the concurrence between the first-, second-, and third-neighbor spins denoted by $1N$, $2N$, and $3N$, respectively [95–97]. We can obtain the expectation values of the density matrix elements for these cases as

$$\begin{aligned} X^{+}_{n,n+1} &= f_0^2 - f_1^2, \\ X^{+}_{n,n+2} &= f_0^2 - f_2^2, \\ X^{+}_{n,n+3} &= f_0^2 - f_3^2, \\ Z_{n,n+1} &= f_1, \\ Z_{n,n+2} &= f_2 - 2f_0 f_2 + 2f_1^2, \\ Z_{n,n+3} &= 4\big(f_1^3 - 2f_0 f_1 f_2 + f_2^2 f_1 + f_0^2 f_3 \\ &\quad - f_1^2 f_3 + f_1 f_2 - f_0 f_3\big) + f_3, \end{aligned} \tag{A5}$$

and

$$\begin{aligned} Y^{+}_{n,m} &= Y^{-}_{n,m} = f_0 - X^{+}_{n,m}, \\ X^{-}_{n,m} &= 1 - 2f_0 + X^{+}_{n,m}, \end{aligned} \tag{A6}$$

where the function f_r $(r = m - n)$ is defined as

$$f_r = \langle c^{\dagger}_{n} c_m \rangle = \frac{1}{N} \sum_{k \in \lambda} e^{i[k(m-n)]}. \tag{A7}$$

We show the concurrence of spin pairs at different distances in Figs. 5(a)–5(c). For $1N$ and $2N$ pairs, Figs. 5(a) and 5(b) show that they are separable in PM and SL-II phases. The magnetic field does not affect this state until $h = 0.0$, where the SL-II phase transitions to the SL-I phase. The entanglement then

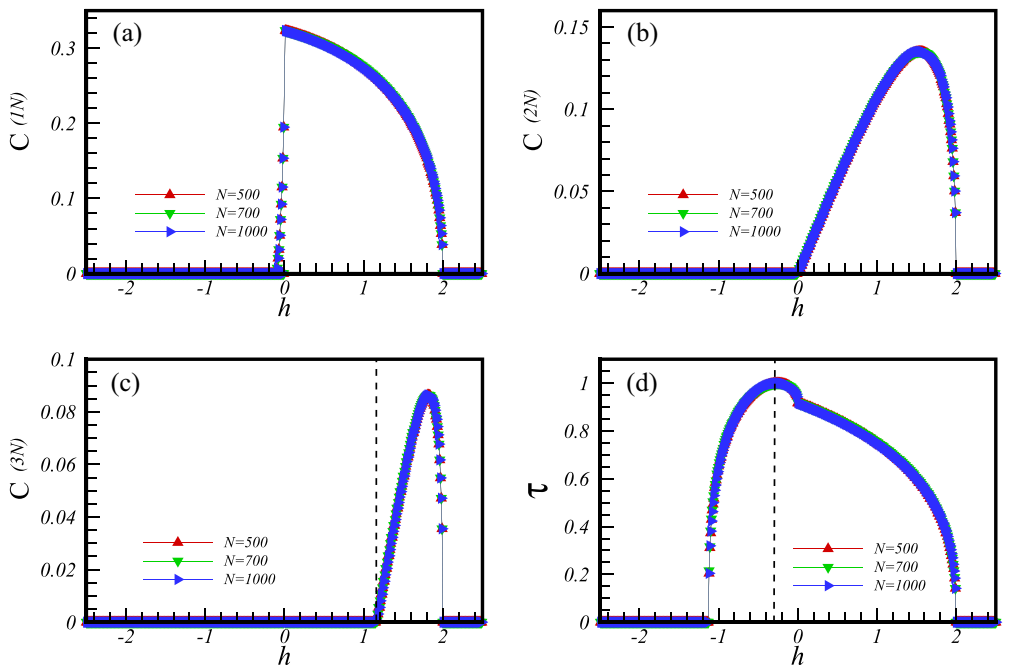

FIG. 5. Concurrence $\mathcal{C}$ as a function of the magnetic field between (a) $1N$, (b) $2N$, and (c) $3N$ pairs of spin. (d) Plot of the one-tangle as a function of the magnetic field, for chain sizes $N = 500$, 700, and 1000 in the presence of TSI, $\alpha = 2$.

drops to zero again at the boundary between SL-I and PM phases. For $3N$ pairs, Fig. 5(c) shows that the magnetic field can entangle them at $h = 1.25$. This value of the magnetic field corresponds to one of the minima in the l_1-norm diagram.

In order to explore the entanglement between one spin and the rest of the chain, the quantity one-tangle is calculated. It is defined as [98]

$$\tau\left(\rho_n^1\right) = 4\det\left(\rho_n^1\right) = \tfrac{1}{4} - \left\langle S_n^z\right\rangle^2, \tag{A8}$$

where ρ_n^1 is the one-site reduced density matrix

$$\rho_n^1 = \begin{pmatrix} \frac{1}{2} + \left\langle S_n^z\right\rangle & 0 \\ 0 & \frac{1}{2} - \left\langle S_n^z\right\rangle \end{pmatrix} \tag{A9}$$

and $\langle S_n^z\rangle$ is the magnetization along the z component. We show the one-tangle calculated analytically as a function of the magnetic field in Fig. 5(d). We see that the one-tangle reaches its maximum value of one at $h = -0.25$, which coincides with a minimum in the l_1-norm diagram. A value of one for the one-tangle means that the one spin is maximally entangled with the rest of the system and its reduced density matrix is a maximally mixed state. This implies that the one spin has no local information and its quantum state is completely determined by its correlations with the other spins. Another minimum in the l_1-norm diagram occurs at $h = 0.65$, indicating a distinct type of quantum correlation in the system that is not captured by concurrence and one-tangle measures.

Our results suggest that the l_1-norm can reveal important features of the quantum critical points, quantum correlations, and coherence of the system by detecting minimum points in its value.

[1] W.-M. Zhang, D. H. Feng, and R. Gilmore, Rev. Mod. Phys. **62**, 867 (1990).
[2] B. C. Sanders, J. Phys. A: Math. Theor. **45**, 244002 (2012).
[3] L. Pezzé, A. Smerzi, M. K. Oberthaler, R. Schmied, and P. Treutlein, Rev. Mod. Phys. **90**, 035005 (2018).
[4] L. Li, Q.-W. Wang, S.-Q. Shen, and M. Li, Phys. Rev. A **103**, 012401 (2021).
[5] T. Baumgratz, M. Cramer, and M. B. Plenio, Phys. Rev. Lett. **113**, 140401 (2014).
[6] A. Streltsov, G. Adesso, and M. B. Plenio, Rev. Mod. Phys. **89**, 041003 (2017).
[7] J. M. Radcliffe, J. Phys. A: Gen. Phys. **4**, 313 (1971).
[8] M. Kitagawa and M. Ueda, Phys. Rev. A **47**, 5138 (1993).
[9] D. J. Wineland, J. J. Bollinger, W. M. Itano, F. L. Moore, and D. J. Heinzen, Phys. Rev. A **46**, R6797 (1992); D. J. Wineland, J. J. Bollinger, W. M. Itano, and D. J. Heinzen, *ibid.* **50**, 67 (1994).
[10] For a review see J. Ma, X. Wang, C. P. Sun, and F. Nori, Phys. Rep. **509**, 89 (2011).
[11] V. Giovannetti, S. Lloyd, and L. Maccone, Science **306**, 1330 (2004).
[12] A. André, A. S. Sørensen, and M. D. Lukin, Phys. Rev. Lett. **92**, 230801 (2004).
[13] C. Gross, T. Zibold, E. Nicklas, J. Estéve, and M. K. Oberthaler, Nature (London) **464**, 1165 (2010).
[14] E. Pedrozo-Peñafiel, S. Colombo, C. Shu, A. F. Adiyatullin, Z. Li, E. Mendez, B. Braverman, A. Kawasaki, D. Akamatsu, Y. Xiao, and V. Vuletić, Nature (London) **588**, 414 (2020).
[15] J. Franke, S. R. Muleady, R. Kaubruegger, F. Kranzl, R. Blatt, A. M. Rey, M. K. Joshi, and C. F. Roos, Nature (London) **621**, 740 (2023).
[16] A. Sørensen, L.-M. Duan, J. I. Cirac, and P. Zoller, Nature (London) **409**, 63 (2001).
[17] A. S. Sørensen and K. Mølmer, Phys. Rev. Lett. **86**, 4431 (2001).
[18] X. Wang and B. C. Sanders, Phys. Rev. A **68**, 012101 (2003).
[19] J. K. Korbicz, O. Gühne, M. Lewenstein, H. Häffner, C. F. Roos, and R. Blatt, Phys. Rev. A **74**, 052319 (2006).
[20] J. Estéve, C. Gross, A. Weller, S. Giovanazzi, and M. K. Oberthaler, Nature (London) **455**, 1216 (2008).
[21] Z. Ren, W. Li, A. Smerzi, and M. Gessner, Phys. Rev. Lett. **126**, 080502 (2021).
[22] J. Feng, E. O. Ilo-Okeke, A. N. Pyrkov, A. Askitopoulos, and T. Byrnes, Phys. Rev. A **104**, 013318 (2021).
[23] J. Vidal, G. Palacios, and R. Mosseri, Phys. Rev. A **69**, 022107 (2004).
[24] W.-F. Liu, J. Ma, and X. Wang, J. Phys. A: Math. Theor. **46**, 045302 (2013).
[25] S. Dusuel and J. Vidal, Phys. Rev. Lett. **93**, 237204 (2004).
[26] J. Ma and X. Wang, Phys. Rev. A **80**, 012318 (2009).
[27] I. Frerot and T. Roscilde, Phys. Rev. Lett. **121**, 020402 (2018).
[28] V. Makhalov, T. Satoor, A. Evrard, T. Chalopin, R. Lopes, and S. Nascimbene, Phys. Rev. Lett. **123**, 120601 (2019).
[29] H. Bao, J. Duan, S. Jin, X. Lu, P. Li, W. Qu, M. Wang, I. Novikova, E. E. Mikhailov, K.-F. Zhao, K. Mølmer, H. Shen, and Y. Xiao, Nature (London) **581**, 159 (2020).
[30] K. Hayashida, T. Makihara, N. M. Peraca, D. F. Padilla, H. Pu, J. Kono, and M. Bamba, Sci. Rep. **13**, 2526 (2023).
[31] I. Frérot, M. Fadel, and M. Lewenstein, Rep. Prog. Phys. **86**, 114001 (2023).
[32] L. Xin, M. Barrios, J. T. Cohen, and M. S. Chapman, Phys. Rev. Lett. **131**, 133402 (2023).
[33] S. J. van Enk and O. Hirota, Phys. Rev. A **64**, 022313 (2001).
[34] C. Wang, Y. Y. Gao, P. Reinhold, R. W. Heeres, N. Ofek, K. Chou, C. Axline, M. Reagor, J. Blumoff, K. M. Sliwa, L. Frunzio, S. M. Girvin, L. Jiang, M. Mirrahimi, M. H. Devoret, and R. J. Schoelkopf, Science **352**, 1087 (2016).
[35] Z. Wang, Z. Bao, Y. Wu, Y. Li, W. Cai, W. Wang, Y. Ma, T. Cai, X. Han, J. Wang, Y. Song, L. Sun, H. Zhang, and L. Duan, Sci. Adv. **8**, eabn1778 (2022).
[36] T. Q. Dat and T. M. Duc, Int. J. Theor. Phys. **59**, 3206 (2020).
[37] M. Mansour, Z. Dahbi, M. Essakhi, and A. Salah, Int. J. Theor. Phys. **60**, 2156 (2021).
[38] P. S. Yan, L. Zhou, W. Zhong, and Y. B. Sheng, Front. Phys. **17**, 21501 (2022).
[39] M. A. Perlin, C. Qu, and A. M. Rey, Phys. Rev. Lett. **125**, 223401 (2020).

[40] T. Comparin, F. Mezzacapo, M. Robert-de-Saint-Vincent, and T. Roscilde, Phys. Rev. Lett. **129**, 113201 (2022).
[41] M. Block, B. Ye, B. Roberts, S. Chern, W. Wu, Z. Wang, L. Pollet, E. J. Davis, B. I. Halperin, and N. Y. Yao, arXiv:2301.09636.
[42] G. Bornet, G. Emperauger, C. Chen *et al.*, Nature (London) **621**, 728 (2023).
[43] M. Suzuki, Phys. Lett. A **34**, 91 (1971); Prog. Theor. Phys. **46**, 1337 (1971).
[44] I. Titvinidze and G. I. Japaridze, Eur. Phys. J. B **32**, 383 (2003).
[45] P. Lou, W.-C. Wu, and M.-C. Chang, Phys. Rev. B **70**, 064405 (2004).
[46] J. K. Pachos and M. B. Plenio, Phys. Rev. Lett. **93**, 056402 (2004).
[47] B. Horstmann, J. I. Cirac, and T. Roscilde, Phys. Rev. A **76**, 043625 (2007).
[48] O. Derzhko, T. Krokhmalskii, J. Stolze, and T. Verkholyak, Phys. Rev. B **79**, 094410 (2009).
[49] W. W. Cheng and J.-M. Liu, Phys. Rev. A **82**, 012308 (2010).
[50] Y.-C. Li and H.-Q. Lin, Phys. Rev. A **83**, 052323 (2011).
[51] R. Jafari and S. Mahdavifar, Prog. Theor. Exp. Phys. **2014**, 43I02 (2014).
[52] G. Zhang and Z. Song, Phys. Rev. Lett. **115**, 177204 (2015).
[53] T. M. Carrijo, A. T. Avelar, and L. C. Céleri, J. Phys. B: At. Mol. Opt. Phys. **48**, 125501 (2015).
[54] W.-L. You, Y.-C. Qiu, and A. M. Oleś, Phys. Rev. B **93**, 214417 (2016).
[55] U. Divakaran, S. Sharma, and A. Dutta, Phys. Rev. E **93**, 052133 (2016).
[56] M. Tahvili and S. Mahdavifar, Physica A **466**, 21 (2017).
[57] Z. Shadman, H. Cheraghi, and S. Mahdavifar, Physica A **512**, 1128 (2018).
[58] Z. Noorinezhad, B. Haghdoust, M. R. Abolhassani, M. Ilkhani, and S. Mahdavifar, J. Supercond. Nov. Magn. **32**, 3873 (2019).
[59] M.-L. Hu, Y.-Y. Gao, and H. Fan, Phys. Rev. A **101**, 032305 (2020).
[60] S. Fu, X. Li, and S. Luo, Phys. Rev. A **106**, 062405 (2022).
[61] E. R. Caianiello and S. Fubini, Nuovo Cimento **9**, 1218 (1952).
[62] S.-A. Cheong and C. L. Henley, Phys. Rev. B **69**, 075111 (2004).
[63] I. Peschel, J. Phys. A: Math. Gen. **36**, L205 (2003).
[64] G. Vidal, J. I. Latorre, E. Rico, and A. Kitaev, Phys. Rev. Lett. **90**, 227902 (2003).
[65] I. Peschel and V. Eisler, J. Phys. A: Math. Theor. **42**, 504003 (2009).
[66] I. Peschel, Braz. J. Phys. **42**, 267 (2012).
[67] C. H. Bennett, H. J. Bernstein, S. Popescu, and B. Schumacher, Phys. Rev. A **53**, 2046 (1996).
[68] A. Kitaev and J. Preskill, Phys. Rev. Lett. **96**, 110404 (2006).
[69] N. Laflorencie, Phys. Rep. **646**, 1 (2016).
[70] A. Bergschneider, V. M. Klinkhamer, J. H. Becher, R. Klemt, L. Palm, G. Zurn, S. Jochim, and P. M. Preiss, Nat. Phys. **15**, 640 (2019).
[71] S.-S. Deng, S.-J. Gu, and H.-Q. Lin, Phys. Rev. B **74**, 045103 (2006).
[72] P. Lou and J. Yong Lee, Phys. Rev. B **74**, 134402 (2006).
[73] K.-W. Sun and Q.-H. Chen, Phys. Rev. B **80**, 174417 (2009).
[74] P. Calabrese and J. Cardy, J. Stat. Mech. (2004) P06002.
[75] M. B. Hastings, J. Stat. Mech. (2007) P08024.
[76] P. Hyllus, W. Laskowski, R. Krischek, C. Schwemmer, W. Wieczorek, H. Weinfurter, L. Pezze, and A. Smerzi, Phys. Rev. A **85**, 022321 (2012).
[77] G. Tóth, Phys. Rev. A **85**, 022322 (2012).
[78] A. Burchardt, J. Czartowski, and K. Życzkowski, Phys. Rev. A **104**, 022426 (2021); A. Burchardt, arXiv:2204.13441.
[79] R. Islam, R. Ma, Philipp M. Preiss, M. Eric Tai, A. Lukin, M. Rispoli, and M. Greiner, Nature (London) **528**, 77 (2015).
[80] J. I. Latorre, E. Rico, and G. Vidal, Quantum Inf. Comput. **4**, 48 (2004).
[81] B.-Q. Jin and V. E. Korepin, J. Stat. Phys. **116**, 79 (2004).
[82] S. F. Huelga, C. Macchiavello, T. Pellizzari, A. K. Ekert, M. B. Plenio, and J. I. Cirac, Phys. Rev. Lett. **79**, 3865 (1997).
[83] B. M. Escher, R. L. de Matos Filho, and L. Davidovich, Nat. Phys. **7**, 406 (2011).
[84] V. Giovannetti, S. Lloyd, and L. Maccone, Nat. Photonics **5**, 222 (2011).
[85] E. Davis, G. Bentsen, and M. Schleier-Smith, Nat. Photon. **116**, 053601 (2016).
[86] H. Yu, Y. Luo, and W. Yao, Phys. Rev. A **84**, 032337 (2011).
[87] R. J. Sewell, M. Koschorreck, M. Napolitano, B. Dubost, N. Behbood, and M. W. Mitchell, Phys. Rev. Lett. **109**, 253605 (2012).
[88] A. A. Batista, Phys. Rev. E **86**, 051107 (2012).
[89] V. Guarrera, R. Gartman, G. Bevilacqua, and W. Chalupczak, Phys. Rev. Res. **3**, L032015 (2021).
[90] T. Hernández Yanes, G. Žlabys, M. Płodzień, D. Burba, M. M. Sinkevičienė, E. Witkowska, and G. Juzeliūnas, Phys. Rev. B **108**, 104301 (2023).
[91] C. H. Bennett, D. P. DiVincenzo, J. A. Smolin, and W. K. Wootters, Phys. Rev. A **54**, 3824 (1996).
[92] S. A. Hill and W. K. Wootters, Phys. Rev. Lett. **78**, 5022 (1997).
[93] W. K. Wootters, Phys. Rev. Lett. **80**, 2245 (1998).
[94] O. F. Syljuåsen, Phys. Rev. A **68**, 060301(R) (2003).
[95] L. Amico, R. Fazio, A. Osterloh, and V. Vedral, Rev. Mod. Phys. **80**, 517 (2008).
[96] F. K. Fumani, S. Nemati, S. Mahdavifar, and A. H. Darooneh, Physica A **445**, 256 (2016).
[97] F. K. Fumani, S. Nemati, and S. Mahdavifar, Ann. Phys. (Berlin) **533**, 2000384 (2021).
[98] L. Amico, A. Osterloh, F. Plastina, R. Fazio, and G. M. Palma, Phys. Rev. A **69**, 022304 (2004).